Neuropsychopharmacology (2014) 39, 895–906

www.neuropsychopharmacology.org

Sub-Anesthetic Ketamine Modulates Intrinsic BOLD Connectivity Within the Hippocampal-Prefrontal Circuit in the Rat

Natalia Gass*[,1], Adam James Schwarz[2,3], Alexander Sartorius[1,4], Esther Schenker[5], Celine Risterucci[6], Michael Spedding[5], Lei Zheng[1,7], Andreas Meyer-Lindenberg[4] and Wolfgang Weber-Fahr[1]

[1]Department of Neuroimaging, Central Institute of Mental Health, Medical Faculty Mannheim, University of Heidelberg, Mannheim, Germany; [2]Translational Medicine, Eli Lilly, Indianapolis, IN, USA; [3]Department of Psychological and Brain Sciences, Indiana University, Bloomington, IN, USA; [4]Department of Psychiatry and Psychotherapy, Central Institute of Mental Health, Medical Faculty Mannheim, University of Heidelberg, Mannheim, Germany; [5]Neuroscience Drug Discovery Unit, Institut de Recherches Servier, Croissy s/Seine, France; [6]CNS Biomarker, Pharmaceuticals Division, F Hoffmann-La Roche, Basel, Switzerland; [7]Experimental Radiation Oncology, University Medical Center Mannheim, University of Heidelberg, Mannheim, Germany

Dysfunctional connectivity within the hippocampal-prefrontal circuit (HC-PFC) is associated with schizophrenia, major depression, and neurodegenerative disorders, and both the hippocampus and prefrontal cortex have dense populations of *N*-methyl-D-aspartate (NMDA) receptors. Ketamine, a potent NMDA receptor antagonist, is of substantial current interest as a mechanistic model of glutamatergic dysfunction in animal and human studies, a psychotomimetic agent and a rapidly acting antidepressant. In this study, we sought to understand the modulatory effect of acute ketamine administration on functional connectivity in the HC-PFC system of the rat brain using resting-state fMRI. Sprague–Dawley rats in four parallel groups ($N = 9$ per group) received either saline or one of three behaviorally relevant, sub-anesthetic doses of S-ketamine (5, 10, and 25 mg/kg, s.c.), and connectivity changes 15- and 30-min post-injection were studied. The strongest effects were dose- and exposure-dependent increases in functional connectivity within the prefrontal cortex and in anterior–posterior connections between the posterior hippocampus and retrosplenial cortex, and prefrontal regions. The increased prefrontal connectivity is consistent with ketamine-induced increases in HC-PFC electroencephalographic gamma band power, possibly reflecting a psychotomimetic aspect of ketamine's effect, and is contrary to the data from chronic schizophrenic patients suggesting that ketamine effect does not necessarily parallel the disease pattern but might rather reflect a hyperglutamatergic state. These findings may help to clarify the brain systems underlying different dose-dependent behavioral profiles of ketamine in the rat. *Neuropsychopharmacology* (2014) **39,** 895–906; doi:10.1038/npp.2013.290; published online 20 November 2013

Keywords: ketamine; functional connectivity; hippocampal-prefrontal; preclinical

INTRODUCTION

The hippocampal-prefrontal circuit (HC-PFC), one of the key pathways mediating cognition and memory, is affected in several psychiatric and neurodegenerative disorders, with dysfunctional connectivity within this circuit being increasingly detected in schizophrenia and major depression, and Alzheimer's disease (Goveas *et al*, 2011; Hasler and Northoff, 2011; Zhou *et al*, 2008). In patients with paranoid schizophrenia, functional connectivity as measured by low-frequency blood oxygenation level-dependent (BOLD) oscillations has been found to be in the absence of any task (Rotarska-Jagiela *et al*, 2010; Zhou *et al*, 2008). In contrast, persistent increases in HC-PFC connectivity has been observed during working memory tasks in schizophrenic patients, subjects at risk, and subjects with first-episode psychosis (Crossley *et al*, 2009; Meyer-Lindenberg *et al*, 2005).

The hippocampus and prefrontal cortex have dense populations of *N*-methyl-D-aspartate (NMDA) receptors. Ketamine, a potent NMDA receptor antagonist, is of substantial current interest both as a psychotomimetic agent (Javitt *et al*, 2012) and a rapidly acting antidepressant, effective in treatment-resistant depressive patients (Zarate *et al*, 2006). Furthermore, ketamine (and other NMDA receptor antagonists) are widely studied in both healthy human volunteers and laboratory animals and represent a translatable pharmacological model of glutamatergic dysfunction in psychiatric disorders (Large, 2007). The neurobiological substrates of the effects of these compounds have begun to be investigated in both rodents and humans

*Correspondence: Dr N Gass, Department of Neuroimaging, Central Institute of Mental Health, Medical Faculty Mannheim, University of Heidelberg, J5, Mannheim 68159, Germany, Tel: +49 0621 17032966, E-mail: natalia.gass@zi-mannheim.de
Received 3 June 2013; revised 21 August 2013; accepted 18 September 2013; accepted article preview online 18 October 2013

using neuroimaging techniques (Doyle *et al*, 2013; Gozzi *et al*, 2008). Recently, the effects of ketamine on resting-state BOLD connectivity have been demonstrated in humans (Driesen *et al*, 2013; Niesters *et al*, 2012; Scheidegger *et al*, 2012), but remain to be elucidated in preclinical species.

This study represents the first investigation of the effects of acute ketamine administration on BOLD functional connectivity in the rat. We assessed three doses (5, 10, 25 mg/kg s.c.) covering a range that has been shown to elicit cognitive, behavioral, imaging, electrophysiological, and neurotransmitter signal changes in a number of studies (Kamiyama *et al*, 2011; Littlewood *et al*, 2006; Lorrain *et al*, 2003; Phillips *et al*, 2012). We focused on the HC-PFC network as a key hypothesized substrate of cognitive and emotional deficits in central nervous system disorders such as schizophrenia (Godsil *et al*, 2013) and following our recent characterization of the HC-PFC connectivity signature in the rat brain (Schwarz *et al*, 2013) that provides a foundation for investigating perturbations of this pathway by drug and/or endophenotype.

MATERIALS AND METHODS

Thirty-six Sprague–Dawley male rats (368–447 g; Janvier Laboratories, Le Genest-St-Isle, France) were used for fMRI experiments. All animals were housed under controlled conditions (19–23 °C, 40–60% humidity) on a 12:12 h light–dark cycle (lights on at 0700 hours).

All procedures were conducted according to the regulations covering animal experimentation within the European Union (European Communities Council Directive 86/609/EEC) and within the German Animal Welfare Act. Experiments were approved by the German animal welfare authorities (Regierungspräsidium Karlsruhe).

MRI Acquisition

Experiments were conducted at a 94/20 Bruker Biospec MRI scanner (9.4 T; Bruker BioSpec, Ettlingen, Germany) with Avance III hardware, BGA12S gradient system with the maximum strength of 705 mT/m, and running Paravision 5.1 software. Transmission and reception were accomplished using a linear whole-body volume transmitter coil combined with an anatomically shaped four-channel receive-only coil array for the rat brain. Rats were anesthetized with 4% isoflurane (Baxter Deutschland GmbH, Unterschleissheim, Germany) in a mixture of N_2 (70%) and O_2 (30%). After positioning in the scanner (head first, prone), isoflurane at $\sim$2.5% was supplied for adjustments. Then, a bolus of 0.5 ml medetomidine solution (Domitor, Janssen-Cilag, Neuss; 0.07 mg/kg s.c.) was injected; isoflurane was slowly discontinued within the next 10 min, after which a continuous infusion of medetomidine solution was started at 0.14 mg/kg/h rate. Breathing and cardiac rates were monitored using a respiration pad placed beneath the chest (Small Animal Instruments, NY) and a pulse oximeter attached to the hindpaw, respectively. Signals were recorded (10-ms resolution) using a signal breakout module (Small Animal Instruments) and a four-channel recorder (Velleman NV, Gavere, Belgium) together with the scanner trigger pulses for each measured brain volume.

The resting-state fMRI (rs-fMRI) time series were acquired using an echo-planar imaging (EPI) sequence with the following parameters: repetition time/echo time (TR/TE) 1700/17.5 ms, flip angle 60°, 1 segment, 29 coronal slices (ascending slice order), 96×96 imaging matrix, field of view $35 \times 35\,mm^2$, slice thickness 0.5 mm with 0.2 mm inter-slice gap, 300 acquisitions over 8.5 min. The in-plane voxel dimension was 0.365 mm and the slice stack covered the brain from the cerebellum to the posterior olfactory bulb.

Experimental Design

The experimental design comprised four parallel groups of $N = 9$ rats each. In three of the groups, S-ketamine (Ketanest, Pfizer Pharma GmbH, Berlin, Germany) was injected s.c. at one of three doses (5, 10, or 25 mg/kg) dissolved in saline (total volume 1 ml/kg). The fourth group received the same volume of vehicle (saline). As the first investigation into the effects of ketamine on functional connectivity in the rat, this was an exploratory study. As such, no formal power calculation was performed. As 7–10 animals per group is typical of rodent fMRI studies, the group size of $N = 9$ per dose in our study was judged sufficient to detect the direction and effect size of the main effects of ketamine and to yield more specific hypotheses to be tested in subsequent confirmatory studies.

The MRI acquisition protocol for each animal comprised a FieldMap and three rs-fMRI time series. The first (baseline) rs-fMRI series was acquired approximately 20 min after the start of medetomidine continuous infusion. The ketamine/saline injection was then performed immediately after acquiring this first rs-fMRI data set, which is 28.5 min after the start of medetomidine continuous infusion and a respective discontinuation of isoflurane supply. The second EPI sequence started at 15 min after the ketamine/vehicle injection and the third—at 30-min post-injection. We selected these two time points to profile the expected peak period of post-injection pharmacodynamic effects based on gamma power changes from electrophysiology measurements after s.c. ketamine injection (Phillips *et al*, 2012) and the relatively rapid pharmacokinetics of the ketamine exposure (which has a peak exposure in the brain within 15 min of s.c. injection; paper in preparation).

At the end of each experiment (within 50–80 min after ketamine/vehicle injection), a blood sample (4.5–6 ml) was taken from each rat by cardiac puncture to determine exposure to ketamine and levels of its major metabolite norketamine. Sample analysis was performed using a mass spectrometry assay by Advion Bioanalytical Labs (Quintiles, Indianapolis, IN; further details are provided in Supplementary Material).

Image Preprocessing

Preprocessing was performed as described previously (for details, see Gass *et al*, 2012). In brief, the EPI time series images were corrected for magnetic field (B_0) inhomogeneities using acquired FieldMap sequences (SPM8 http://www.fil.ion.ucl.ac.uk/spm/software/spm8/). To minimize the

effect of movement on the signal intensities, the estimated movement parameter vectors were regressed out from each voxel (FSL, version 4.1. http://www.fmrib.ox.ac.uk/fsl). Afterward, respiratory and cardiac signals were filtered out from each voxel using Aztec software (van Buuren *et al*, 2009). A slice-timing correction was then applied to the images using SPM8. We used this order of preprocessing steps as it has been shown to be the most optimal in terms of minimizing temporal standard deviation (Jones *et al*, 2008). The time courses were then band-pass filtered (0.01–0.1 Hz; Analysis of Functional Neuroimages (AFNI) version 2). Finally, the functional data were spatially normalized (SPM8) to a rat brain template with co-registered anatomical atlas positioned in the Paxinos stereotactic coordinate system (Schwarz *et al*, 2006) using a three-step process: (1) creation of a mean image from all time series and normalization of all images to this grand mean image, (2) normalization of the grand mean image to the template, and (3) normalization of all images from step 1 to the template using the transformation matrix from step (2).

Region-of-Interest Correlation Analysis

Coupling between predefined regions of interest (ROI) was assessed using two spatial sampling schemes. For the primary analysis, the brain was parcellated into 10 midline or bilateral hippocampal and cortical brain regions corresponding to established atlas structures (Schwarz *et al*, 2006; Figure 1). The cortical regions included infralimbic, prelimbic, orbitofrontal, cingulate (areas 1 and 2), and retrosplenial cortices; the hippocampus was subdivided into anterodorsal, posterodorsal, ventral, and subiculum/dentate gyrus parts of the hippocampus (Gass *et al*, 2012). In a secondary analysis, 19 midline or bilateral $0.6 \times 0.6 \times 0.8$ mm ROIs centered on specified stereotactic coordinates were defined as in our previous characterization of functional connectivity (Schwarz *et al*, 2013). This enabled the conclusions of the first analysis to be tested with a different (sparse) spatial sampling scheme and provides a direct link to the previous work.

The mean time course from each ROI was extracted for each rs-fMRI time series. All-pairs correlation coefficients were then calculated, and converted to z-scores $z(r)$ using Fisher's r-to-z transformation $(0.5 \times \ln[(1+r)/(1-r)])$. Within each subject, the 15- and 30-min post-injection values of $z(r)$ were each normalized to the corresponding pre-injection baseline values: $\delta z_{15} = z_{15} - z_{\mathrm{pre}}$ and $\delta z_{30} = z_{30} - z_{\mathrm{pre}}$, using each animal as its own within-scanning session control in order to maximize sensitivity to acute connectivity changes following compound injection.

To assess the dose-response effect of ketamine, each ROI–ROI pair in the resulting δz matrices was analyzed across the two post-injection time points and the four treatment conditions using an ANOVA model with dose (0, 5, 10, 25 mg/kg ketamine) and time point (15- and 30-min post-injection) as factors. A false discovery rate correction of $q = 0.05$ was applied to accommodate the multiple ROI pairs tested.

Further, pharmacokinetic–pharmacodynamic (PK–PD) relationships between ketamine plasma levels and changes in connectivity were assessed by fitting an $E_{\max}$ model $(\delta z = \delta z_{\min} + (\delta z_{\max} - \delta z_{\min})/(1 + 10^{(\log(\mathrm{EC50}) - [\mathrm{ket}])})$ to ketamine concentrations ([ket]) and δz values. A robust fit was not achieved for all ROI pairs; values from selected successful fits are reported to illustrate the consistency between dose- and exposure-response profiles. Plasma ketamine levels were not corrected for the time difference between PK sample measurement and the rs-fMRI data acquisition.

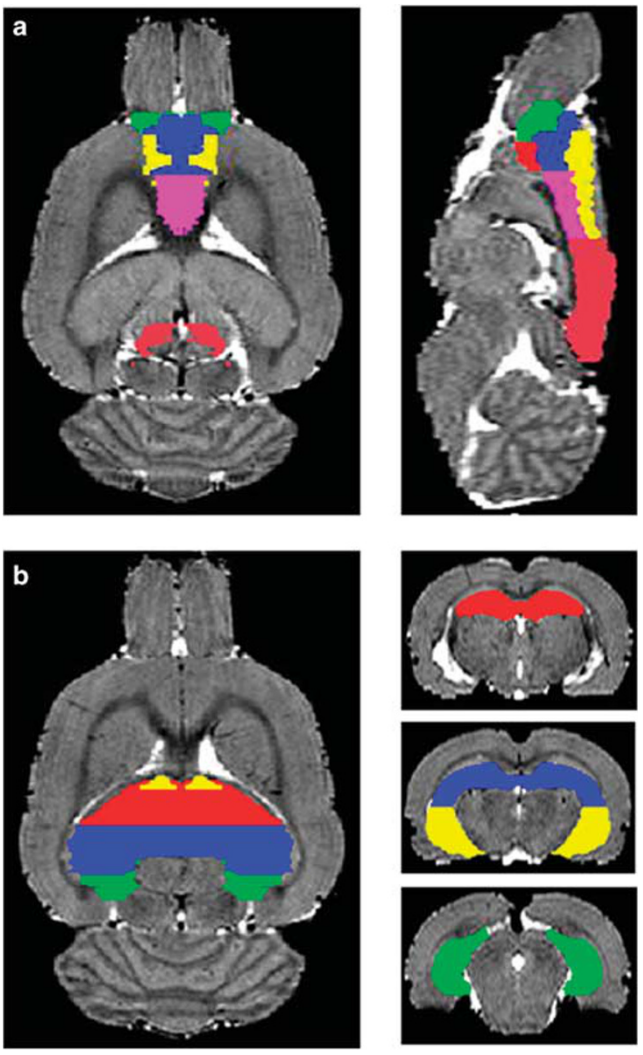

Figure 1 Brain masks used in ROI–ROI and seed-based analyses. Color coding: (a) red—infralimbic cortex; blue—prelimbic cortex; green—orbitofrontal cortex; yellow—cingulate cortex, area 1; magenta—cingulate cortex area 2; pink—retrosplenial cortex. (b) Red—anterodorsal hippocampus; blue—posterodorsal hippocampus; green—subiculum/dentate gyrus; yellow—ventral hippocampus.

Seed Region Analyses

The extracted time courses of the prefrontal (infralimbic, prelimbic, and orbitofrontal) and all hippocampal regions were used for seed-based functional connectivity analysis (SPM8). A mean time course of the seed region was extracted from each normalized, unsmoothed time series; then the data were smoothed by 0.8 mm (approximately two voxels in-plane). Correlation coefficients r were calculated for the extracted time courses voxel-wise and transformed

Table 1 Ketamine and Norketamine Concentrations Measured in Plasma by Experimental Group

Experimental group	Mean [SD] (min-max) plasma concentration (ng/ml)	
	Ketamine	Norketamine
Vehicle	3.76 [6.93] (BQL[a]–21.36)	4.08 [12.23] (BQL[b]–37.76)
5 mg/kg	282.33 [164.52] (131.99–637.59)	305.03 [172.06] (139.46–659.58)
10 mg/kg	601.81 [181.83] (391.56–893.39)	527.72 [259.08] (329.13–1065.74)
25 mg/kg	1693.87 [475.92] (922.1–2516.49)	1333.01 [585.78] (800.88–2377.84)

[a]5/9 animals had ketamine levels below quantifiable level (BQL) of 1.00 ng/ml.
[b]6/9 animals had norketamine levels below quantifiable level (BQL) of 1.00 ng/ml.

to Fisher z-scores as above. Next, each of the post-injection z-scores maps was normalized to pre-injection baseline by subtracting the pre-injection z-value from each corresponding voxel (creating δz maps). These δz maps were fed into two second level analyses: (1) an ANOVA analysis using a contrast $[-3, -1, 1, 3]$ to assess dose response, and (2) a regression analysis using individual subject ketamine plasma levels as predictors, to assess dependence on peripheral drug exposure. These analyses were performed for each of the δz_{15} and δz_{30} maps.

The obtained statistic images were cluster corrected for multiple comparisons using FSL (height thresholds: $t = 2.449$ for ANOVA; $t = 2.441$ for regression analysis; $p_{\text{cluster}} = 0.01$).

Effect of Ketamine on Cardiac Frequency

To evaluate potential confounding effects on functional connectivity because of changes in heart rate, we calculated mean cardiac frequencies over time windows corresponding to the three rs-fMRI acquisitions. First, the cardiac data were band-pass filtered (2.5–6.0 Hz) and Fourier transformed. The resulting spectra showing the cardiac frequency distribution were Gauss-fitted to extract representative mean values. The calculated mean cardiac frequencies were analyzed using a general linear model (GLM) for repeated measurements with dose as between-subject factor. The repeated-measures GLM did not show a significant dose effect ($p = 0.493$). Also *post-hoc* contrasts of the cardiac mean frequencies for the different ketamine doses were not significant compared with saline.

RESULTS

Ketamine Plasma Concentrations

Ketamine plasma levels evidenced a linear dependence on dose (Table 1). In the vehicle group, concentrations were below the quantifiable limit (1 ng/ml) in 5/9 animals. Plasma levels of the major metabolite, norketamine, also increased linearly with dose and were highly correlated with ketamine levels ($r^2 = 50\%$).

ROI–ROI Correlations

We first examined the effects of ketamine on functional connectivity using the set of predefined atlas ROIs. The ANOVA analysis over each ROI pair (Figure 2a) revealed significant effects of dose on connectivity that involved (1) connections within prefrontal and cingulate regions and (2) antero–posterior connections from hippocampal regions and the retrosplenial cortex to prefrontal and cingulate regions. Overall, the strongest effects were observed between different regions of the prefrontal and cingulate cortices, and between the retrosplenial cortex and the cingulate cortex area 2. Dose-dependent alterations were observed between all prefrontal and cingulate cortex pairs (with the exception of the infralimbic cortex to cingulate cortex area 1 connection). A second main feature we observed was an altered connectivity between the subiculum/dentate gyrus of the hippocampus and three prefrontal regions (infralimbic cortex, orbitofrontal cortex, and cingulate cortex area 2). Finally, significant effects of dose were also observed between the infralimbic cortex and both the retrosplenial cortex and posterodorsal hippocampus. The effect of post-injection time point (15 or 30 min) was not significant for any ROI pair.

In all ROI pairs exhibiting a significant effect of dose, the effect of ketamine manifested as an increased correlation strength at both time points, although the magnitude and profile of the dose–response relationships varied across region pairs (Figure 2b). In some cases, near maximal connectivity change was observed at the 5 mg/kg dose (eg, prelimbic to infralimbic cortex, prelimbic to orbitofrontal cortex), whereas in others the effect increased more strongly with dose, with the connectivity change at 25 mg/kg substantially greater than those at the lower doses (eg, prelimbic to cingulate cortex area 2, subiculum/dentate gyrus to orbitofrontal cortex). Figure 2c illustrates, in an anatomically anchored node-to-node view, the ROI–ROI pairs exhibiting a significant effect of ketamine dose on functional connectivity.

PK/PD modeling revealed exposure–response relationships consistent with the dose–response behavior. Regions with connectivity changes that were near-maximal at the 5 mg/kg dose exhibited $E_{\max}$ model fits that approached a plateau at the higher plasma ketamine concentrations (eg, prelimbic to infralimbic cortex (Figure 3a); $\log(EC50) \sim 2.2$–2.4, $EC_{50} = 166$ ng/ml at 15 min and 234 ng/ml at 30 min). Conversely, regions with more steeply increasing connectivity changes as a function of dose exhibited $E_{\max}$ curves that were further right-shifted (eg, infralimbic to cingulate cortex area 2 (Figure 3b); $\log(EC50) \sim 3.4$, $EC_{50} = 2730$ ng/ml at 15 min and 2627 ng/ml at 30 min).

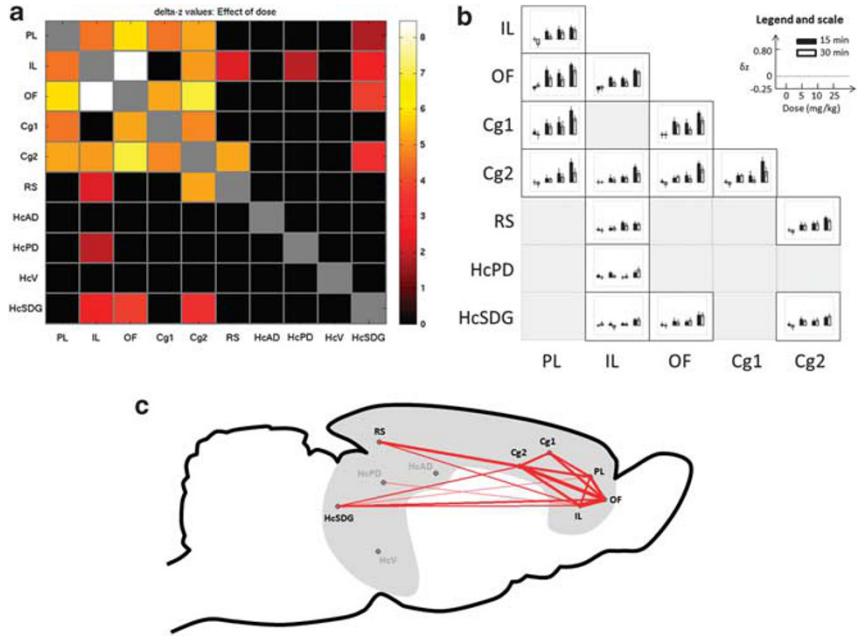

Figure 2 (a) ROI–ROI pairs for which the main effect of dose was significant (two-way ANOVA (dose and time point as factors); FDR: $q < 0.05$); color bar indicates statistical significance as $-\log_{10}(p)$; black squares: ROI pairs not achieving statistical significance. (b) ROI–ROI pair dose–response profiles for correlation coefficient δz changes; shown only for cells identified as significant. (c) Sagittal view of the node-to-node connections within the hippocampal-prefrontal system exhibiting a significant effect of ketamine dose (cf. (a)). Thicker lines indicate statistically stronger effects. Cg1, cingulate cortex, area 1; Cg2, cingulate cortex, area 2; HcAD, hippocampus, anterodorsal; HcPD, hippocampus, posterodorsal; HcSDG, hippocampus, subiculum and dentate gyrus; HcV, hippocampus, ventral; IL, infralimbic cortex; OF, orbitofrontal cortex; PL, prelimbic cortex; RS, retrosplenial cortex.

Results with the coordinate ROI set (19×19 ROIs) were consistent with those described above, namely a widespread effect of dose corresponding to increased functional connectivity within the prefrontal cortex and in more specific connections between hippocampal and prefrontal regions (Supplementary Material).

Whole-Brain Seed Region Analyses

We next performed whole-brain voxel-wise seed region analyses to assess the effects of ketamine, with respect to pre-defined hippocampal and prefrontal seeds (Table 2). For most of the seeds, the strongest modulatory effects of ketamine were localized to the prefrontal cortex.

Among the hippocampal seeds, the strongest finding was an increased connectivity of the subiculum/dentate gyrus with prefrontal (prelimbic cortex, orbitofrontal cortex, and cingulate cortex area 1) and insular cortices at both post-injection time points. This was observed with respect to both dose and ketamine plasma concentrations (Figure 4a). For the other hippocampal regions, significant changes in connectivity were stronger at 30-min post-injection. The anterodorsal and posterodorsal hippocampi had increased connectivity with prelimbic, retrosplenial, and insular cortices (*vs* both dose and ketamine plasma levels), and the ventral hippocampus showed increased connectivity with the caudate-putamen as a function of ketamine plasma levels at 30 min only.

Among the prefrontal regions, the strongest result was observed with respect to infralimbic cortex and comprised an increased connectivity with orbital cortex and cingulate cortex area 2 at 15 min, with the prelimbic cortex at both time points and with the postsubiculum at 30-min post-injection. A similar increased connectivity with prefrontal cortex was obtained for the orbitofrontal seed and prelimbic seeds.

DISCUSSION

We demonstrated that acute ketamine challenge induces dose- and exposure-dependent increases in functional connectivity within the HC-PFC system in the rat brain. Specifically, we observed (1) an increased connectivity between most pairs of regions within the prefrontal and cingulate cortices, and (2) an increased anterior–posterior connectivity between the retrosplenial cortex and posterior regions of the hippocampus, and regions in the prefrontal cortex.

Although rs-fMRI is well established in humans and has been shown to be sensitive to pharmacological modulation, consistent intrinsic connectivity networks have only recently been demonstrated in the rat, and pharmacological effects on rs-fMRI are only beginning to be characterized in the rodent (Gass *et al*, 2012). This study moves this field forward in several respects. First, we elucidated the effects of ketamine—one of the most widely used compounds in behavioral research and pharmacological screening—on functional connectivity in the rat brain. This provides a preclinical analog of rs-fMRI studies that are increasingly performed in humans and will help to determine the translational viability of functional connectivity measures in this pharmacological model. Second, we evaluated a range of behaviorally active doses and assessed compound

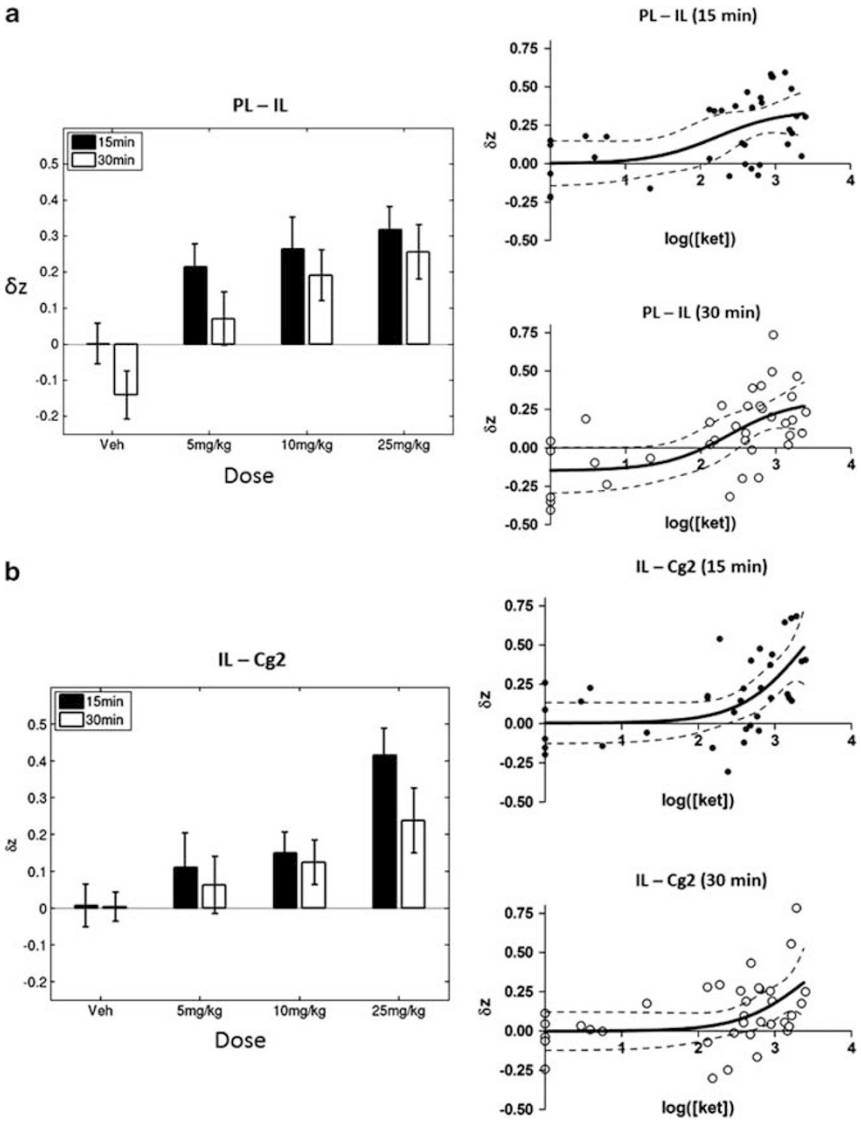

Figure 3 Illustration of consistent dose–response and exposure–response relationships. (a) Change in normalized correlation coefficients (δz) between prelimbic (PL) and infralimbic (IL) cortices across treatment conditions (left) and ketamine exposure levels (right) (15- and 30-min post-injection). (b) Change in normalized correlation coefficients (δz) between IL cortex and cingulate cortex area 2 (Cg2) across treatment conditions (left) and ketamine exposure levels (right) (15- and 30-min post-injection).

exposure in plasma, enabling dose–response and PK–PD relationships to be evaluated. This is standard practice in most pharmacological assays but remains under-utilized in fMRI studies.

The connectivity changes we observed were in region pairs consistent with the strongest connections within this network reported in our previous study (Schwarz *et al*, 2013); namely, between subregions of the prefrontal and cingulate cortices and between the posterior (subiculum) region of the hippocampus and the prefrontal cortex. This latter functional coupling matches the anatomical projection reaching from the posterior CA1 and subiculum regions of the hippocampus to the infralimbic, prelimbic, and anterior cingulate cortices (Godsil *et al*, 2013). We also applied the same ANOVA model to the set of coordinate-based ROIs used in our previous study (Schwarz *et al*, 2013), and found very similar results, with the strongest emergent finding being a widespread dose-dependent increase in connectivity between anterior seeds with more restricted modulation of correlations between the hippocampus and prefrontal cortex. Although obtained from the same data set and thus not an independent sample, this secondary analysis nevertheless confirms that the primary findings of this study are also observed with a sparse and more focal anatomical sampling, and thus are not an artifact of our particular choice of ROIs.

Our finding of increased functional coupling following ketamine infusion is directly consistent with a recent study (Driesen *et al*, 2013) of ketamine effects on rs-fMRI in humans, where a widespread increase in brain connectivity (quantified as overall node connectivity) was reported, although HC-PFC interactions were not specifically examined. Two other recent studies (Niesters *et al*, 2012; Scheidegger *et al*, 2012) examining ketamine effects on

Table 2 Loci of Peak Voxels and Cluster Center of Gravity for Significant Clusters Obtained from Seed-Connectivity Analysis (ANOVA and Regression Analysis (Correlation with Ketamine Exposure)) at 15- and 30-Min Post-Injection

Seed region	Model	Time point	Cluster	Number of voxels in cluster	*p*-value	$-LOG_{10}(P)$	T_{MAX}	Peak voxel of cluster			Cluster center of gravity			Anatomical localization	
								X (M–L) (mm)	Y (D–V) (mm)	Z (A–P) (mm)	X (M–L) (mm)	Y (D–V) (mm)	Z (A–P) (mm)	Peak voxel	Cluster center of gravity
HcAD	**Dose (ANOVA)**	**15 min**	—	—	—	—	—	—	—	—	—	—	—	—	—
		30 min	3	311	0.0004	3.45	6.31	2.8	−3.87	1.52	1.9	−4.45	3.37	CPu	CI
			2	181	0.0096	2.02	5.68	−4.87	−6.43	2.25	−4.34	−5.47	2.52	DI	DI
			1	143	0.0285	1.54	4.33	3.53	−0.59	−5.41	0.44	−0.67	−6.0	VI	RSD
	PK (regression)	**15 min**	2	99	0.0177	1.75	4.01	−4.5	−1.68	3.35	−4.03	−1.52	2.99	MI	Fr3
			1	97	0.0195	1.71	3.42	3.89	−3.14	4.44	4.9	−2.42	2.37	MI	SIDZ
		30 min	3	159	0.0078	2.11	5.51	3.89	−0.59	−5.41	0.78	−0.63	−5.86	VI	RSD
			2	148	0.0113	1.95	5.72	−4.87	−6.43	2.25	−4.72	−6.43	1.29	DI/AID	DI
			1	107	0.0492	1.31	4.33	3.53	−4.6	4.08	2.68	−3.97	4.36	AID	AIV/AID
HcPD	**Dose (ANOVA)**	**15 min**	1	183	0.0010	3.02	4.68	3.16	−1.68	−1.03	4.69	−2.46	−0.62	SIHL	SIFL/SIDZ
		30 min	3	572	1.4e–05	4.85	5.66	0.97	−0.95	4.08	0.64	−4.1	3.21	M2	PL
			2	280	0.0027	2.57	5.85	−4.5	−6.06	1.89	−4.0	−5.53	2.23	DI	GI
			1	278	0.0028	2.55	4.34	−5.96	−3.51	−1.4	−5.31	−2.94	−1.48	SIBF	SIBF
	PK (regression)	**15 min**	—	—	—	—	—	—	—	—	—	—	—	—	—
		30 min	3	500	2.95e–05	4.53	4.98	−2.31	−1.68	4.44	0.76	−3.5	3.61	M2	PL
			2	427	0.0001	3.96	5.68	−4.87	−6.06	1.89	−4.16	−5.97	1.81	GI	AID/VCI
			1	192	0.0149	1.83	4.45	−0.85	−2.41	−0.67	−0.04	−2.34	−0.54	Cg2/Cg1	Cg2/Cg1
HcSDG	**Dose (ANOVA)**	**15 min**	5	274	0.0008	3.08	4.29	0.24	−4.6	4.81	0.57	−3.84	3.89	MO	PL
			4	231	0.0024	2.61	4.77	2.8	−2.41	−0.67	2.75	−2.18	−0.56	SIHL	SIHL
			3	222	0.0031	2.51	4.64	−2.68	−4.24	0.42	−1.96	−2.23	1.65	CPu	MI/M2
			2	139	0.0316	1.5	4.99	−3.04	−3.87	4.81	−3.63	−4.78	3.1	DLO	DI
			1	128	0.0442	1.35	5.46	−6.69	−3.87	−2.86	−6.41	−3.96	−2.71	SIUlp	SIUlp
		30 min	3	610	5.3e–06	5.28	6.43	−4.14	−5.33	2.25	−1.68	−4.85	2.88	GI	CI
			2	468	5.91e–05	4.23	4.85	−3.41	−1.68	−2.86	−4.44	−2.15	−1.37	SITr	SIDZ
			1	228	0.0068	2.17	4.03	2.8	−1.32	1.52	3.04	−0.98	−0.46	MI	SIHL
	PK (regression)	**15 min**	2	749	5.96e–08	7.22	5.01	−3.77	−5.7	1.89	−0.83	−3.18	2.39	DCI	Cg2
			1	136	0.0329	1.48	4.18	2.07	−3.14	−1.4	3.93	−2.37	−0.33	SIHL	SIFL
		30 min	1	1983	7.11e–13	12.1	6.65	−4.14	−5.7	1.89	−0.81	−3.99	1.59	GI	Cg2
HcV	**Dose (ANOVA)**	**15 min**	—	—	—	—	—	—	—	—	—	—	—	—	—
		30 min	—	—	—	—	—	—	—	—	—	—	—	—	—
	PK (regression)	**15 min**	—	—	—	—	—	—	—	—	—	—	—	—	—
		30 min	1	86	0.0303	1.52	4.28	−1.95	−3.14	−0.67	−2.73	−3.88	−0.03	SIHL	CPu
IL	**Dose (ANOVA)**	**15 min**	2	3451	2.05e–17	16.7	7.79	−1.95	−3.87	4.44	−0.81	−2.68	1.22	LO	Cg2
			1	204	0.0247	1.61	4.13	6.45	−2.78	−2.49	6.23	−3.9	−3.58	SIBF	S2
		30 min	2	1200	2e–09	8.7	6.33	−0.12	−4.24	4.08	0.15	−3.27	3.41	PL	PL
			1	688	2.26e–06	5.64	5.02	0.6	−0.22	−2.13	−2.68	−1.21	−1.36	M2	SIHL
	PK (regression)	**15 min**	1	1603	1.93e–13	12.7	6.22	−1.22	−1.32	2.98	−0.15	−2.83	2.56	M2	PL
		30 min	3	1027	4.52e–10	9.34	5.61	−0.12	−4.24	4.08	−0.04	−3.17	3.2	PL	PL
			2	144	0.0262	1.58	5.84	−2.68	−3.87	−6.51	−2.65	−3.38	−6.43	SuG	Post
			1	133	0.0366	1.44	3.77	−3.41	−0.22	1.52	−2.84	−0.69	0.27	MI	SIHL

Table 2 (Continued)

Seed region	Model	Time point	Cluster	Number of voxels in cluster	*p*-value	$-LOG_{10}(P)$	T_{MAX}	Peak voxel of cluster			Cluster center of gravity			Anatomical localization	
								X (M–L) (mm)	Y (D–V) (mm)	Z (A–P) (mm)	X (M–L) (mm)	Y (D–V) (mm)	Z (A–P) (mm)	Peak voxel	Cluster center of gravity
OF	**Dose (ANOVA)**	**15 min**	1	2927	1.52e–15	14.8	7.13	0.24	−4.24	2.62	0.01	−2.8	1.53	PL	Cg2
		30 min	1	1794	3.05e–12	11.5	5.5	0.24	−3.87	2.62	−0.29	−2.91	1.38	PL	Cg2
	PK (regression)	**15 min**	2	2083	3.02e–14	13.5	6.15	−4.14	−6.06	1.89	0.01	−2.86	2.19	DI	Cg2
			1	162	0.0326	1.49	4.34	−2.68	−0.22	−4.68	−2.74	−0.39	−4.6	V2ML	V2ML
		30 min	2	2439	8.28e–14	13.1	6.46	0.24	−3.87	2.62	−0.46	−2.72	1.28	PL	Cg2
			1	285	0.0052	2.29	4.67	5.35	−3.14	−7.97	3.95	−3.39	−7.19	V2L	Post
PL	**Dose (ANOVA)**	**15 min**	3	2825	5.77e–15	14.2	6.5	0.6	−4.24	2.98	0.11	−2.49	2.18	PL	Cg2
			2	225	0.0176	1.75	5.96	−7.06	−3.87	−2.13	−6.59	−4.19	−1.99	S1Ulp	S1BF
			1	176	0.0466	1.33	5.6	−7.06	−6.43	−6.51	−6.12	−4.04	−7.29	PRh	V2L
		30 min	3	1035	6.16e–09	8.21	5.96	0.6	−4.6	2.98	−0.1	−3.37	3.7	PL/IL	PL
			2	612	3.76e–06	5.43	5.82	−2.68	−0.59	1.16	−0.46	−0.44	−0.99	M1	M2
			1	194	0.0131	1.88	4.36	−6.69	−3.14	−2.49	−6.45	−3.58	−1.97	S1BF	S1BF
	PK (regression)	**15 min**	1	2105	3.75e–14	13.4	5.5	−4.14	−6.06	1.89	−0.02	−2.61	2.57	DI	PL
			1*	209	0.0114	1.94	4.37	0.6	−3.87	−2.13	−0.49	−6.58	−2.2	CA3	AM
		30 min	1	2262	4.1e–14	13.4	7.03	2.07	−3.51	4.44	−0.25	−2.34	2.1	CI/LO	Cg1/Cg2

Abbreviations: AID, agranular insular cortex, dorsal part; AIV, agranular insular cortex, ventral part; AM, anteromedial thalamic nucleus; A–P, anteroposterior; CA3, field CA3 of the hippocampus; CPu, caudate-putamen; Cg1, cingulate cortex, area 1; Cg2, cingulate cortex, area 2; CI, claustrum; DCI, dorsal claustrum; DI, dysgranular insular cortex; DLO, dorsolateral orbital cortex; D–V, dorsoventral; Fr3, frontal cortex, area 3; GI, granular insular cortex; HcAD, hippocampus, anterodorsal; HcPD, hippocampus, posterodorsal; HcSDG, hippocampus, subiculum and dentate gyrus; HcV, hippocampus, ventral; IL, infralimbic cortex; LO, lateral orbital cortex; M1, primary motor cortex; M2, secondary motor cortex; M–L, mediolateral; MO, medial orbital cortex; OF, orbitofrontal cortex; PL, prelimbic cortex; Post, postsubiculum; PRh, perirhinal cortex; RSD, retrosplenial dysgranular cortex; S1BF, primary somatosensory cortex, barrel field; S1DZ, primary somatosensory cortex, dysgranular zone; S1FL, primary somatosensory cortex, forelimb region; S1HL, primary somatosensory cortex, hindlimb region; S1Tr, primary somatosensory cortex, trunk region; S1Ulp, primary somatosensory cortex, upper limb region; S2, secondary somatosensory cortex; SuG, superficial gray layer of the superior colliculus; V1, primary visual cortex; V2L, secondary visual cortex, lateral area; V2ML, secondary visual cortex, mediolateral area; V2MM, secondary visual cortex, mediomedial area; VCl, ventral claustrum.

In regression analysis, both positive and negative correlations were calculated; for all seeds except PL only positive correlations were statistically significant and therefore displayed. Negative correlations for PL are marked with asterisk (*). Coordinates are given in the stereotactic space of Paxinos and Watson.

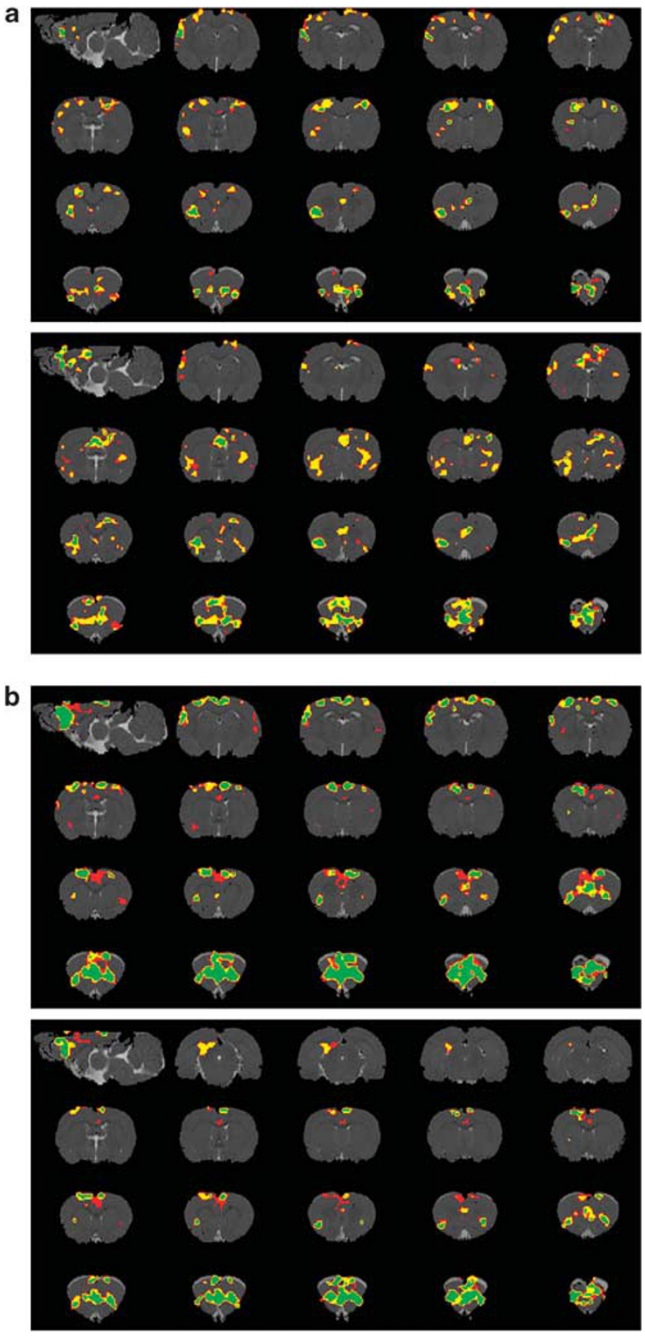

Figure 4 Maps of functional connectivity for (a) subiculum/dentate gyrus; (b) infralimbic cortex. For both (a) and (b) upper panel represents ANOVA dose-response analysis, lower panel—positive correlation with ketamine plasma levels. Coronal slice coverage in z-bregma: (a) −2.4÷4.8 mm for both upper and lower panels, (b) −2.4÷4.8 mm for upper panel; −6.4÷−5.2 mm (upper row) and −0.8÷4.8 mm (from the second to the fourth rows) for lower panel. Color coding: red—15-min post-injection, yellow—30-min post-injection, green—overlap in correlation between 15- and 30-min post-injection. Maps are thresholded at $p = 0.01$.

rs-fMRI in humans were not methodologically consistent with our study. In one (Scheidegger *et al*, 2012), connectivity changes were assessed 24 h following cessation of ketamine infusion, for direct comparison with clinical studies in treatment-resistant depression but quite different to our paradigm in which connectivity changes were assessed during the maximal period of ketamine exposure. In the other (Niesters *et al*, 2012) a different analysis approach (dual regression) was used and connectivity changes with respect to visual and somatosensory networks, not assessed in our work, were reported.

Interestingly, both the increased intra-prefrontal and HC-PFC connectivities are opposite to the pattern seen at rest in paranoid schizophrenic patients (Rotarska-Jagiela *et al*, 2010; Zhou *et al*, 2008). This finding argues against a simplistic interpretation of acute ketamine challenge as a 'schizophrenia model' at the brain system level and favors a more subtle interpretation. As ketamine acutely induces aberrant glutamate cycling and release, it might more specifically model hyperglutamatergic states/traits of schizophrenia. Indeed, some, but not all, patients exhibit elevated glutamate levels—a neurobiological feature that is associated with response to standard dopaminergic treatments (Egerton *et al*, 2012). Elevated glutamate levels are also preferentially associated with the early stages of schizophrenia; moreover (1) the glutamine/glutamate ratio is increased in patients at the early stage but becomes lower than in healthy subjects once the disease reaches its chronic stage (Marsman *et al*, 2013), and (2) ketamine produces cognitive disruption that resembles the data observed in patients with prodromal stage of schizophrenia (Moore *et al*, 2013). Future work to understand these relationships is necessary, for example, through clinical studies of rs-fMRI in early stage *vs* chronic schizophrenic patients and characterization of genetic high-risk rodent models for schizophrenia such as copy number variant mice.

Although ketamine challenge is often interpreted in terms of glutamatergic function, we note that, at the neurochemical level, ketamine also induces elevation of glutamate and several other excitatory neurotransmitters levels, such as norepinephrine, acetylcholine, dopamine, and histamine in the HC-PFC regions (Fell *et al*, 2010; Kubota *et al*, 1999; Lorrain *et al*, 2003; Moghaddam *et al*, 1997; Sato *et al*, 1996), probably by blocking NMDA receptors on GABAergic interneurons and a consequent facilitation of disinhibition (Seamans, 2008) and also when binding to cholinergic, monoaminergic, nicotinic, and muscarinic receptors (Mion and Villevieille, 2013). The resulting disinhibition of cortical and hippocampal neurons drives an increased glucose utilization (Duncan *et al*, 1998) and BOLD image contrast in hippocampal and prefrontal regions in the rat (Chin *et al*, 2011).

The whole-brain seed region analyses indicated that the strongest effects on connectivity with regions in the HC-PFC network were predominantly within this same network. However, several significant effects were observed between HC-PFC regions and structures outside this circuit. A region that consistently showed an increased functional coupling with this circuit was the insular cortex. Functionally, the insula is a versatile brain area involved in visceral sensation (Critchley *et al*, 2004), pain perception (Isnard *et al*, 2011), and social emotions (Immordino-Yang *et al*, 2009) in humans. Insular morphometric changes are consistently found in early psychosis and correlate with psychosis severity (Crespo-Facorro *et al*, 2000). The increased correlations observed between the insula and infralimbic cortex as well as with the hippocampal seeds in the presence

of ketamine could reflect a modulation of the above mentioned functions: changes in body perception, analgesia, and a psychotomimetic effect, all of which are observed following ketamine infusion in humans.

In ROI pairs where the E_{max} model could be reliably estimated, we found a good correspondence between dose–response and exposure–response relationships to ketamine. However, we found evidence that, for the doses tested here, the dose–response relationship was different for different pairs of brain regions. Many of the connections between the prefrontal/anterior cingulate subregions showed near-maximal connectivity changes at the 5 mg/kg dose. In contrast, many of the anterior–posterior connections (eg, subiculum/dentate gyrus or cingulate cortex area 2 to more anterior ROIs) evidenced a more monotonic dose–response with maximal correlation changes observed at the 25 mg/kg dose. One limitation of the study is that the plasma samples were obtained approximately 30–45 min after the rs-fMRI measurements, and so the measured ketamine concentrations could be as much as an order of magnitude less than those during the first rs-fMRI time series. Nevertheless, if a well-behaved decrease in plasma concentration for each subject is assumed, the relative forms of the exposure–response relationships we found (eg, lower exposures required to alter connectivity between prelimbic and infralimbic cortices relative to infralimbic-cingulate cortex area 2 connectivity; Figure 3) should be similar to those that would have been obtained if samples were obtained concurrently with the rs-fMRI measurements, especially as these were highly consistent with dose–response relationships in the same brain region pairs (Figure 3).

Electrophysiological measures relevant to psychiatric disorders, NMDA blockade, and the HC-PFC system suggest some possible neuronal correlates of our observations. The power of gamma oscillations (30–80 Hz), a ubiquitous rhythm hypothesized to integrate neural networks and to have a major role in perception, is enhanced in schizophrenic patients compared with healthy controls (Bandyopadhyaya *et al*, 2011). Also in human and in rat, ketamine induces an increase in baseline gamma power (Pinault, 2008), which most likely results from the blockade of NMDA receptors at GABAergic interneurons, as they have greater sensitivity to NMDA receptor antagonists than pyramidal neurons (Grunze *et al*, 1996). However, the increase in gamma band activity following visual processing and memory tasks is reduced in schizophrenia and following ketamine in healthy subjects (Grutzner *et al*, 2013), implying that while resting-state coherence may be increased, neuronal plasticity involving NMDA receptors is impaired in these key circuits (Godsil *et al*, 2013). Given the strong correlation between gamma band oscillations and BOLD connectivity in humans (Tagliazucchi *et al*, 2012), these findings may provide a neuronal underpinning for our findings in this study. Although the effect of time point (15 *vs* 30-min post-injection) was not significant in the ROI–ROI analysis, changes at 30 min were qualitatively slightly lower than those at 15 min, very consistent with the time-profile of gamma band power changes over the visual cortex reported following 10 mg/kg ketamine challenge, which peaked at approximately 15–20 min and were only slightly lower by 30 min (Phillips *et al*, 2012). However, it has yet to be demonstrated more explicitly that the types of connectivity observed in our study reflect gamma activation.

It should be noted that acute and long-term effects of ketamine on functional connectivity likely differ. The delayed effects of ketamine are suggested to underlie the antidepressant action and were not directly assessed in this study. Although brain-derived neurotrophic factor (BDNF) protein translation rises in the hippocampus and cortex as fast as 30-min post-ketamine injection, and BDNF is likely to be crucial for ketamine antidepressant effect (Autry *et al*, 2011), the improvement in mood is delayed and takes place $\sim$2 h after ketamine administration in depressed patients (Zarate *et al*, 2006), which is beyond the time points that we studied. Indeed, in contrast to the results of our study, at 24 h after ketamine administration a reduction of functional connectivity between the posterior cingulate cortex and dorsomedial prefrontal cortex, pregenual anterior cingulate cortex and medioprefrontal cortex was observed, opposite to the pattern observed in depressed patients (Scheidegger *et al*, 2012).

We additionally measured the plasma concentration of ketamine's major metabolite, norketamine, which showed a steady increase with the increasing dose and correlated with ketamine plasma levels. Norketamine has been shown to positively correlate with post-ketamine stimulus-evoked somatosensory responses (Cornwell *et al*, 2012). Although norketamine could also have some effects on resting-state brain connectivity, future studies should examine closer its neural effects as well as its further metabolite dehydronorketamine.

This study was performed using light medetomidine anesthesia, raising the possibility of a confounding interaction with ketamine. It is known that alpha-2 adrenoreceptor agonists are able to reduce the hyperadrenergic state produced by ketamine (Levanen *et al*, 1995). However, medetomidine is widely used in a number of laboratories for the investigation of resting-state connectivity in the rodent, and is favored based on evidence that it presumably has a minimal effect on neural activity (Nasrallah *et al*, 2012): rs-fMRI correlations are more localized in contrast to other anesthetics, for example, isoflurane (Nasrallah *et al*, 2012) and it reveals functional connectivity maps in the rat that are more comparable to what is seen in humans (Williams *et al*, 2010). Studies of the interaction between anesthetics and pharmacological MRI responses to NMDA receptor antagonists (ketamine and phencyclidine) have suggested a dependence of the valence of the response on anesthesia (Hodkinson *et al*, 2012), although this is likely to be due to a combined (anesthetic + NMDA receptor antagonist) dose effect (Gozzi *et al*, 2008), where at higher combined doses the overall effect is one of sedation (depressed cortical activity) rather than the excitatory profile observed at lower doses of anesthesia and/or NMDA receptor antagonist challenge. The fact that we did not observe a change in valence at the highest ketamine dose used in this study argues that the maintenance level of medetomidine used here was sufficiently light to avoid this major interaction confound. Together with the observation that our results are similar to the effects produced by ketamine on metabolic activity in conscious rats as well as consistent with human data (Driesen *et al*, 2013), we consider that drug–anesthetic interaction was not a dominant factor in the results of this study.

This study was the first to examine the effects of ketamine on resting state functional connectivity in the rat. As such, it was exploratory in nature; our main hypothesis before the study was that functional connectivity between the hippocampus and the prefrontal cortex would be altered, and we did find evidence supporting this. These findings yield more specific hypotheses to be tested in independent, confirmatory experiments: for example, that ketamine increases functional connectivity within the prefrontal cortex and between the subiculum area of the hippocampus and prefrontal regions, and that differential dose–response profiles are observed between these two sets of region pairs. To aid appropriate powering of such confirmatory studies, we report effect sizes for the atlas ROI pairs in the Supplementary Material (Supplementary Tables S1–S6).

In conclusion, ketamine-induced alterations in HC-PFC functional coupling corresponding to changes in behavior, EEG, and neurotransmission provide further evidence of rs-fMRI as a sensitive probe of central pharmacological effects in preclinical species. The finding of increased connectivity between the hippocampus and prefrontal cortex contrary to the data from schizophrenic patients suggests that ketamine effect does not necessarily parallel the disease pattern and might rather reflect a hyperglutamatergic state.

FUNDING AND DISCLOSURE

AJS is an employee and shareholder of Eli Lilly, CR is an employee of F Hoffmann-La Roche, MS and ES are employees of Instituts de Recherches Servier. AM-L received consultant fees and travel expenses from Alexza Pharmaceuticals, AstraZeneca, Bristol Myers Squibb, Defined Health, Decision Resources, Desitin Arzneimittel, Elsevier, F Hoffmann-La Roche, Gerson Lehrmann Group, Groupo Ferrer, Les Laboratoires Servier, Lilly Deutschland, Lundbeck Foundation, Outcome Sciences, Outcome Europe, Pricespective, Roche Pharma, speaker's fees from Abbott, AstraZeneca, BASF, Bristol-Myers Squibb, Glaxo SmithKline, Janssen Cilag, Lundbeck, Pfizer Pharma, and Servier Deutschland.

ACKNOWLEDGEMENTS

The authors thank Felix Hörner and Claudia Falfan-Melgoza for their excellent technical assistance. NEWMEDS—the research leading to these results, has received support from the Innovative Medicine Initiative Joint Undertaking under Grant Agreement No. 115008 of which resources are composed of European Federation of Pharmaceutical Industries and Associations (EFPIA) in-kind contribution and financial contribution from the European Union's Seventh Framework Programme (FP7/2007–2013). Also the work was supported by the BMBF (01EW1110) in the frame of ERA-Net NEURON.

REFERENCES

Autry AE, Adachi M, Nosyreva E, Na ES, Los MF, Cheng PF *et al* (2011). NMDA receptor blockade at rest triggers rapid behavioural antidepressant responses. *Nature* **475**: 91–95.

Bandyopadhyaya D, Nizamie SH, Pradhan N, Bandyopadhyaya A (2011). Spontaneous gamma coherence as a possible trait marker of schizophrenia-An explorative study. *Asian J Psychiatr* **4**: 172–177.

Chin CL, Upadhyay J, Marek GJ, Baker SJ, Zhang M, Mezler M *et al* (2011). Awake rat pharmacological magnetic resonance imaging as a translational pharmacodynamic biomarker: metabotropic glutamate 2/3 agonist modulation of ketamine-induced blood oxygenation level dependence signals. *J Pharmacol Exp Ther* **336**: 709–715.

Cornwell BR, Salvadore G, Furey M, Marquardt CA, Brutsche NE, Grillon C *et al* (2012). Synaptic potentiation is critical for rapid antidepressant response to ketamine in treatment-resistant major depression. *Biol Psychiatry* **72**: 555–561.

Crespo-Facorro B, Kim J, Andreasen NC, O'Leary DS, Bockholt HJ, Magnotta V (2000). Insular cortex abnormalities in schizophrenia: a structural magnetic resonance imaging study of first-episode patients. *Schizophr Res* **46**: 35–43.

Critchley HD, Wiens S, Rotshtein P, Ohman A, Dolan RJ (2004). Neural systems supporting interoceptive awareness. *Nat Neurosci* **7**: 189–195.

Crossley NA, Mechelli A, Fusar-Poli P, Broome MR, Matthiasson P, Johns LC *et al* (2009). Superior temporal lobe dysfunction and frontotemporal dysconnectivity in subjects at risk of psychosis and in first-episode psychosis. *Hum Brain Mapp* **30**: 4129–4137.

Doyle OM, De Simoni S, Schwarz AJ, Brittain C, O'Daly OG, Williams SC *et al* (2013). Quantifying the attenuation of the ketamine pharmacological magnetic resonance imaging response in humans: a validation using antipsychotic and glutamatergic agents. *J Pharmacol Exp Ther* **345**: 151–160.

Driesen NR, McCarthy G, Bhagwagar Z, Bloch M, Calhoun V, D'Souza DC *et al* (2013). Relationship of resting brain hyperconnectivity and schizophrenia-like symptoms produced by the NMDA receptor antagonist ketamine in humans. *Mol Psychiatry*.

Duncan GE, Moy SS, Knapp DJ, Mueller RA, Breese GR (1998). Metabolic mapping of the rat brain after subanesthetic doses of ketamine: potential relevance to schizophrenia. *Brain Res* **787**: 181–190.

Egerton A, Brugger S, Raffin M, Barker GJ, Lythgoe DJ, McGuire PK *et al* (2012). Anterior cingulate glutamate levels related to clinical status following treatment in first-episode schizophrenia. *Neuropsychopharmacology* **37**: 2515–2521.

Fell MJ, Katner JS, Johnson BG, Khilevich A, Schkeryantz JM, Perry KW *et al* (2010). Activation of metabotropic glutamate (mGlu)2 receptors suppresses histamine release in limbic brain regions following acute ketamine challenge. *Neuropharmacology* **58**: 632–639.

Gass N, Schwarz AJ, Sartorius A, Cleppien D, Zheng L, Schenker E *et al* (2012). Haloperidol modulates midbrain-prefrontal functional connectivity in the rat brain. *Eur Neuropsychopharmacol* **23**: 1310–1319.

Godsil BP, Kiss JP, Spedding M, Jay TM (2013). The hippocampal-prefrontal pathway: The weak link in psychiatric disorders? *Eur Neuropsychopharmacol* **23**: 1165–1181.

Goveas JS, Xie C, Ward BD, Wu Z, Li W, Franczak M *et al* (2011). Recovery of hippocampal network connectivity correlates with cognitive improvement in mild Alzheimer's disease patients treated with donepezil assessed by resting-state fMRI. *J Magn Reson Imaging* **34**: 764–773.

Gozzi A, Schwarz A, Crestan V, Bifone A (2008). Drug-anaesthetic interaction in phMRI: the case of the psychotomimetic agent phencyclidine. *Magn Reson Imaging* **26**: 999–1006.

Grunze HC, Rainnie DG, Hasselmo ME, Barkai E, Hearn EF, McCarley RW *et al* (1996). NMDA-dependent modulation of CA1 local circuit inhibition. *J Neurosci* **16**: 2034–2043.

Grutzner C, Wibral M, Sun L, Rivolta D, Singer W, Maurer K *et al* (2013). Deficits in high- (>60 Hz) gamma-band oscillations

during visual processing in schizophrenia. *Front Hum Neurosci* **7**: 88.

Hasler G, Northoff G (2011). Discovering imaging endophenotypes for major depression. *Mol Psychiatry* **16**: 604–619.

Hodkinson DJ, de Groote C, McKie S, Deakin JF, Williams SR (2012). Differential effects of anaesthesia on the phMRI response to acute ketamine challenge. *Br J Med Med Res* **2**: 373–385.

Immordino-Yang MH, McColl A, Damasio H, Damasio A (2009). Neural correlates of admiration and compassion. *Proc Natl Acad Sci USA* **106**: 8021–8026.

Isnard J, Magnin M, Jung J, Mauguiere F, Garcia-Larrea L (2011). Does the insula tell our brain that we are in pain? *Pain* **152**: 946–951.

Javitt DC, Zukin SR, Heresco-Levy U, Umbricht D (2012). Has an angel shown the way? Etiological and therapeutic implications of the PCP/NMDA model of schizophrenia. *Schizophr Bull* **38**: 958–966.

Jones TB, Bandettini PA, Birn RM (2008). Integration of motion correction and physiological noise regression in fMRI. *Neuroimage* **42**: 582–590.

Kamiyama H, Matsumoto M, Otani S, Kimura SI, Shimamura KI, Ishikawa S *et al* (2011). Mechanisms underlying ketamine-induced synaptic depression in rat hippocampus-medial prefrontal cortex pathway. *Neuroscience* **177**: 159–169.

Kubota T, Anzawa N, Hirota K, Yoshida H, Kushikata T, Matsuki A (1999). Effects of ketamine and pentobarbital on noradrenaline release from the medial prefrontal cortex in rats. *Can J Anaesth* **46**: 388–392.

Large CH (2007). Do NMDA receptor antagonist models of schizophrenia predict the clinical efficacy of antipsychotic drugs? *J Psychopharmacol* **21**: 283–301.

Levanen J, Makela ML, Scheinin H (1995). Dexmedetomidine premedication attenuates ketamine-induced cardiostimulatory effects and postanesthetic delirium. *Anesthesiology* **82**: 1117–1125.

Littlewood CL, Jones N, O'Neill MJ, Mitchell SN, Tricklebank M, Williams SC (2006). Mapping the central effects of ketamine in the rat using pharmacological MRI. *Psychopharmacology (Berl)* **186**: 64–81.

Lorrain DS, Baccei CS, Bristow LJ, Anderson JJ, Varney MA (2003). Effects of ketamine and N-methyl-D-aspartate on glutamate and dopamine release in the rat prefrontal cortex: modulation by a group II selective metabotropic glutamate receptor agonist LY379268. *Neuroscience* **117**: 697–706.

Marsman A, van den Heuvel MP, Klomp DW, Kahn RS, Luijten PR, Hulshoff Pol HE (2013). Glutamate in schizophrenia: a focused review and meta-analysis of (1)H-MRS studies. *Schizophr Bull* **39**: 120–129.

Meyer-Lindenberg AS, Olsen RK, Kohn PD, Brown T, Egan MF, Weinberger DR *et al* (2005). Regionally specific disturbance of dorsolateral prefrontal-hippocampal functional connectivity in schizophrenia. *Arch Gen Psychiatry* **62**: 379–386.

Mion G, Villevieille T (2013). Ketamine pharmacology: an update (pharmacodynamics and molecular aspects, recent findings). *CNS Neurosci Ther* **19**: 370–380.

Moghaddam B, Adams B, Verma A, Daly D (1997). Activation of glutamatergic neurotransmission by ketamine: a novel step in the pathway from NMDA receptor blockade to dopaminergic and cognitive disruptions associated with the prefrontal cortex. *J Neurosci* **17**: 2921–2927.

Moore JW, Cambridge VC, Morgan H, Giorlando F, Adapa R, Fletcher PC (2013). Time, action and psychosis: using subjective time to investigate the effects of ketamine on sense of agency. *Neuropsychologia* **51**: 377–384.

Nasrallah FA, Tan J, Chuang KH (2012). Pharmacological modulation of functional connectivity: alpha2-adrenergic receptor agonist alters synchrony but not neural activation. *Neuroimage* **60**: 436–446.

Niesters M, Khalili-Mahani N, Martini C, Aarts L, van Gerven J, van Buchem MA *et al* (2012). Effect of subanesthetic ketamine on intrinsic functional brain connectivity: a placebo-controlled functional magnetic resonance imaging study in healthy male volunteers. *Anesthesiology* **117**: 868–877.

Phillips KG, Cotel MC, McCarthy AP, Edgar DM, Tricklebank M, O'Neill MJ *et al* (2012). Differential effects of NMDA antagonists on high frequency and gamma EEG oscillations in a neurodevelopmental model of schizophrenia. *Neuropharmacology* **62**: 1359–1370.

Pinault D (2008). N-methyl d-aspartate receptor antagonists ketamine and MK-801 induce wake-related aberrant gamma oscillations in the rat neocortex. *Biol Psychiatry* **63**: 730–735.

Rotarska-Jagiela A, van de Ven V, Oertel-Knochel V, Uhlhaas PJ, Vogeley K, Linden DE (2010). Resting-state functional network correlates of psychotic symptoms in schizophrenia. *Schizophr Res* **117**: 21–30.

Sato K, Wu J, Kikuchi T, Wang Y, Watanabe I, Okumura F (1996). Differential effects of ketamine and pentobarbitone on acetylcholine release from the rat hippocampus and striatum. *Br J Anaesth* **77**: 381–384.

Scheidegger M, Walter M, Lehmann M, Metzger C, Grimm S, Boeker H *et al* (2012). Ketamine decreases resting state functional network connectivity in healthy subjects: implications for antidepressant drug action. *PLoS One* **7**: e44799.

Schwarz AJ, Danckaert A, Reese T, Gozzi A, Paxinos G, Watson C *et al* (2006). A stereotaxic MRI template set for the rat brain with tissue class distribution maps and co-registered anatomical atlas: application to pharmacological MRI. *Neuroimage* **32**: 538–550.

Schwarz AJ, Gass N, Sartorius A, Zheng L, Spedding M, Schenker E *et al* (2013). The low-frequency blood oxygenation level-dependent functional connectivity signature of the hippocampal-prefrontal network in the rat brain. *Neuroscience* **228**: 243–258.

Seamans J (2008). Losing inhibition with ketamine. *Nat Chem Biol* **4**: 91–93.

Tagliazucchi E, von Wegner F, Morzelewski A, Brodbeck V, Laufs H (2012). Dynamic BOLD functional connectivity in humans and its electrophysiological correlates. *Front Hum Neurosci* **6**: 339.

van Buuren M, Gladwin TE, Zandbelt BB, van den Heuvel M, Ramsey NF, Kahn RS *et al* (2009). Cardiorespiratory effects on default-mode network activity as measured with fMRI. *Hum Brain Mapp* **30**: 3031–3042.

Williams KA, Magnuson M, Majeed W, LaConte SM, Peltier SJ, Hu X *et al* (2010). Comparison of alpha-chloralose, medetomidine and isoflurane anesthesia for functional connectivity mapping in the rat. *Magn Reson Imaging* **28**: 995–1003.

Zarate CA Jr, Singh JB, Carlson PJ, Brutsche NE, Ameli R, Luckenbaugh DA *et al* (2006). A randomized trial of an N-methyl-D-aspartate antagonist in treatment-resistant major depression. *Arch Gen Psychiatry* **63**: 856–864.

Zhou Y, Shu N, Liu Y, Song M, Hao Y, Liu H *et al* (2008). Altered resting-state functional connectivity and anatomical connectivity of hippocampus in schizophrenia. *Schizophr Res* **100**: 120–132.

Supplementary Information accompanies the paper on the Neuropsychopharmacology website (http://www.nature.com/npp)